Chapter 15

Landslides

Hawa Mahar in Jaipur, Rajastan, India. This was a place for ladies of Maharaja's court to look at a parade in the street. This is a very thin building in contrast with its width as seen here.

15.1 Earthquake-Induced Landslides

Earthquake is one of the major causes of landslides. Keefer (1984) summarized past records to classify them and also to show the maximum distance to landslides for varying seismic magnitudes. He also showed that the minimum earthquake magnitude to cause landslides is M_L = 4.0 according to US records. It seems, however, that this number depends on local geology as well as the annual rainfall.

Figure 15.1 shows an overall view of a large landslide which occurred near Galdian village during the 1990 Manjil earthquake (M = 7.3) in Iran (Ishihara et al. 1992). The soil type in the slip plane was clayey as indicated by the exposed slip plane (Fig. 15.2). Some part of the sliding soil was mixed with water and formed a mud flow (Fig. 15.3). It is not uncommon that sliding mass is significantly fluidized and reaches an unexpectedly long distance.

Fig. 15.1 Galdian landslide in Iran during the 1990 Manjil earthquake

Fig. 15.2 Exposed slip plane in Galdian landslide

Fig. 15.3 Deposit of fluidized material near landslide in Fig. 15.1

Fig. 15.4 Seismic collapse of Mt. Ontake (photo by Prof. K. Ishihara)

Figure 15.4 shows the collapse in a slope Mt. Ontake during the 1984 Nagano-ken Seibu earthquake. Being a volcano, the body of this mountain was made of debris with water. Thus, it collapsed easily upon shaking, got fluidized, and flowed downstream along a valley. Note further that volcanic slopes are subjected to nonseismic failures as well which are induced by slope steepening due to magma intrusion and hydrothermal excess pore water pressure caused by magma intrusion (Voight and Elsworth, 1997).

It is interesting that the risk of fluidization depends on moisture content of soil. Figure 15.5 indicates a slope failure in the town of Muzaffarabad which was triggered by an earthquake in 2005 that hit North Kashmir of Pakistan. It is important that the soil of the collapsed slope did not travel laterally and many

houses in the small valley were not affected by the soil flow. It seems that this fortunate situation was produced by the dry state of soil. Since the earthquake occurred in dry season (early October), there was not much water in the slope. There is water in subsoil, however, if water is supplied from leaking canal, pipeline, irrigation channel, or reservoir.

The 2005 earthquake in Pakistan showed several interesting features of seismic slope failure. Figure 15.6 demonstrates an example which occurred to the north of Muzaffarabad. The surface of limestone slope was significantly weathered due to temperature change and heavy sunshine, in particular, because of the lack of vegetation and repeated wetting and drying together with freezing in winter. The state of weathering is evidenced in detail by Fig. 15.7.

Failure of surface material may not be so significant in volume as those in Figs. 15.1 and 15.4. It is, however, able to stop local transportation if the fallen debris close a mountain road. Figure 15.6 is an example. The time needed to open the road again is shorter than the case of failure of road embankments (Figs. 14.12, 14.43 and 15.8), because removal of fallen debris is much easier than reconstruction of a fill. Modern construction of highway tries to make a short cut by crossing valleys by means of embankments and bridges. Consequently, a failure of embankment seriously affects the operation of transportation. Conversely, such roads located along slope surface are constructed by cutting slopes and are more stable during earthquakes, although such roads are curved and not good for high-speed transportation.

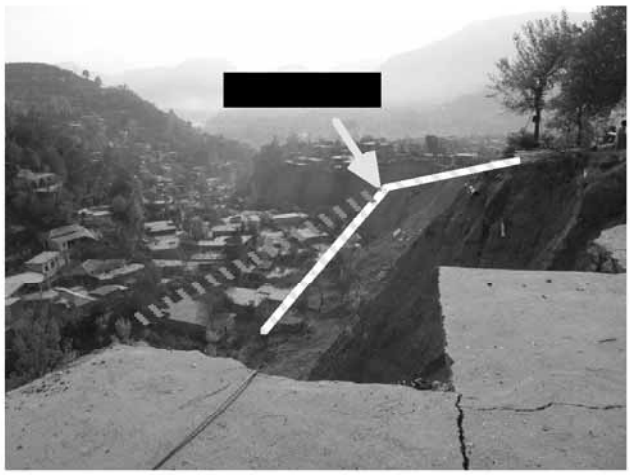

Fig. 15.5 Collapse of dry slope in Muzaffarabad, Pakistan

Fig. 15.6 Surface failure of weathered limestone slope near Muzaffarabad, Pakistan, in 2005

Fig. 15.7 Weathered rock surface in Pakistan, 2005

Fig. 15.8 Collapse of slope surface and road shoulder near Barakot of Pakistan

Ohya slide (大谷崩れ, Fig. 15.9) in Shizuoka Prefecture, Japan, is said to have been caused by the 1707 Hoei (宝永) gigantic earthquake. Since then, the destabilized slope (Fig. 15.10) has been producing

debris flow at heavy rainfall frequently (Imaizumi et al. 2005). Consequently, the bed of the Abe River (安倍川) is filled with cobbles and stones, rising continuously due to sediments (Fig. 15.11). To mitigate this situation, many erosion control dams have been constructed (Fig. 15.12). However, the problem has not yet been solved. Effort is also made to plant trees in the unstable slope (Fig. 15.13). It is noteworthy that decreased discharge of sediment from rivers into the sea has recently resulted in erosion of beaches, making coastal structures less unstable than before. The same problem is found in downstream area of rivers as well where the foundation of bridges is scoured.

Fig. 15.9 Ohya slide in Shizuoka

Fig. 15.10 Unstable mountain slope

Fig. 15.11 Valley of Abe River

Fig. 15.12 Erosion control dams in Abe river channel

Fig. 15.13 Tree planting in unstable Ohya slope

15.2 Yungay City Destroyed by Earthquake-Induced Debris Flow

An earthquake-induced collapse of Snowy Huascaran Mountain (Nevados Huascarán; Fig. 15.14) in Peru in 1970 was characterized by debris which was fluidized when the falling rock and ice were mixed with water and stream deposits. A debris flow thus developed flowed over a small hill and buried the whole city of Yungay, killing over 30,000 people. Figure 15.15 shows the city prior to the disaster; the hill and Mt. Huascarán are seen behind. This debris flow traveled hundreds of kilometers along the channel of Río Santa to finally reach the Pacific Ocean. The total volume of this debris avalanche is assessed to be 50 million m^3 (Plafker et al. 1971). The soil deposit at the ruins of Yungay includes much amount of fines (Fig. 15.16), suggesting that original rocky material was ground into small particles.

Fig. 15.14 Slope of Huascaran Mountain (in August, 1989)

Fig. 15.15 Mt. Huascaran and Yungay City in July, 1965 (Hayakawa, 1967)

Fig. 15.16 Soil at ruin of former Yungay City

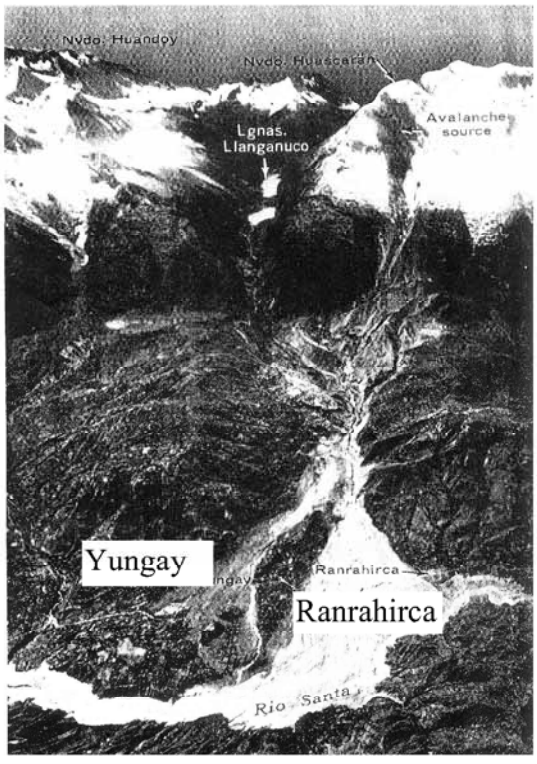

Fig. 15.17 Aerial view of Yungay-Ranrahirca area (Town names were added to original photograph by Plafker et al. 1971)

Figure 15.17 shows the aerial view of the concerned area. The town of Ranrahirca was attacked in 1960 by another flow, while Yungay was protected by a hill. This experience gave the Yungay residents a wrong idea that their town was well protected from such a geohazard. This idea did not work in 1970

when another flow had a greater size.

After this tragedy, the city of Yungay was reconstructed at a safer place. Relocation is the best solution for avoiding natural disasters. It has to be borne in mind, however, that relocated people have to survive by finding new source of income. It is not good that they have to rely on governmental aids forever. Farmers need new agricultural land and fishermen need to go to the sea. This requirement is not always satisfied in relocation programs. Figure 15.18 and 15.19 show a life-aid activity by NGO (Non Governmental Organization) for those who were evacuated from home villages after eruption of Pinatubo volcano and resultant lahar flow (flooding of rain water with volcanic ash deposit); Figs. 15.20 and 15.21 in the Philippines.

Fig. 15.18 Production of hand crafts by Pinatubo refugee people

Fig. 15.19 Aid for self support of Pinatubo refugee people

Fig. 15.20 River bed filled with flooding of lahar from Pinatubo Volcano, the Philippines

Fig. 15.21 Church which was 50% buried by lahar after Pinatubo eruption in the Philippines

15.3 Tsaoling Landslide in Taiwan

The 1999 ChiChi (集集) earthquake in Taiwan triggered many landslides in this geologically young island which was produced by tectonic interaction between Eurasia and Philippine sea plates. Being of the tertiary origin (新世代第三紀), the young rock of the island has not yet developed a stable geological structure. Moreover, the tectonic motion has distorted the rock significantly, developing fractured rock conditions. The high rate of rainfall and erosion have made steep mountain slopes which are prone to instability.

Fig. 15.22 Overall view of Tsaoling landslide

Fig. 15.23 Slip plane after the 1999 quake

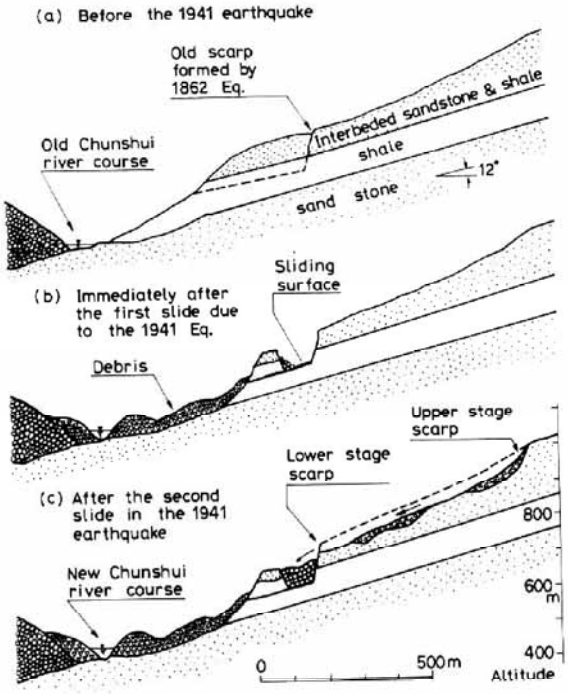

Fig. 15.24 Repeated instability of Tsaoling slope (Ishihara, 1985)

Figure 15.22 illustrates the overall view of the Tsaoling (草嶺) slide which included the total volume of sliding mass greater than 100 million m^3. Of 4 km in width, this amount of sliding mass appears to be one of the greatest seismically induced landslides in the twentieth century. Similar to other landslides during the same earthquake, the Tsaoling slide occurred in an interbedded slope of shale and mud stone. Figure 15.23 shows the slip plane which was seen after the quake (December, 1999). It is important that this slide had developed failure two times during the past earthquakes; the first one in 1862 and the second in 1941 (Fig. 15.24). Another big sliding occurred due to rainfall in

Fig. 15.25 Natural dam after 1999 event

1942 and stopped the flow of river (Kawata, 1943). Being the biggest in the scale, the failure in 1999 was simply a failure of the remaining rock mass.

A big landslide often generates a natural dam. In 1999, the dam lake in Fig. 15.25 was produced. If the natural dam body is narrow, its erosion during high water level and a possible failure may lead to flooding and debris flow. Tabata et al. (2002) made a statistic analysis on landslide-induced natural dams in Japan. The size (length of dam in the direction of river channel) and depth information in Figs. 15.26 and 15.27 may be useful. Noteworthy is that most natural dams in the past failed due to overtopping of water, which led to erosion, and the number of failures due to piping of seepage water (seepage of water removing debris from the body of dam) is small (Fig. 15.28).

Figure 15.29 demonstrates a water channel which was excavated across a natural dam (Terano natural dam, 2004 Niigata-Chuetsu earthquake).

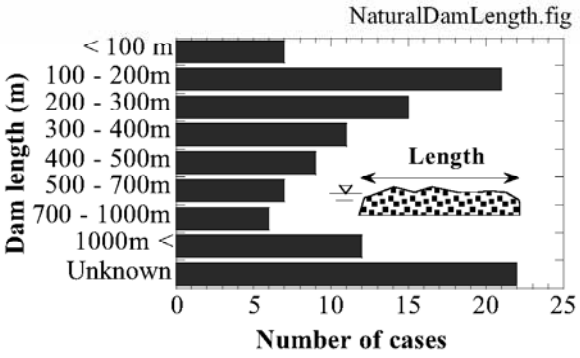

Fig. 15.26 Statistics on length of natural dam in the direction of river channel (after Tabata et al. 2002)

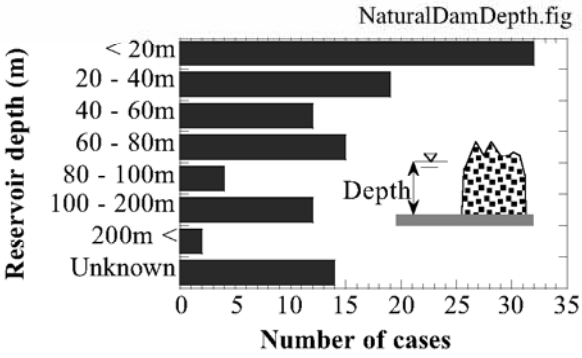

Fig. 15.27 Statistics on depth of reservoir dam produced by natural dam (after Tabata et al. 2002)

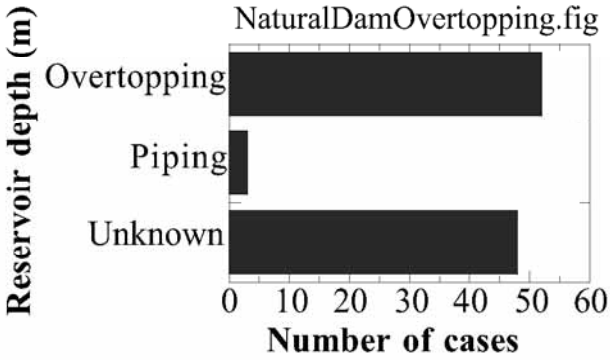

Fig. 15.28 Statistics on cause of failure of natural dams (after Tabata et al. 2002)

Fig. 15.29 Water drainage channel in Terano natural dam in Niigata

Sampling, laboratory shear tests, and stability analyses were performed to understand the Tsaoling landslide triggered by the 1999 Chi-Chi earthquake of Taiwan. Samples were collected from the slip plane (Fig. 15.23) and debris deposits. Figure 15.24 showed the stratification of local geology which is parallel to the slope. Attention was therefore focused on the possibility of a weak layer and a weak interface between two different rocks. The problem was that the slope had already collapsed, making sampling of weak intact materials impossible. It was decided consequently to collect samples from debris deposits of broken rocks as well as the remaining slickenside slip plane (Fig. 15.23). Shear tests were carried out at CRIEPI (Central Research Institute of Electric Power Industry) by using its direct shear device, see Fig. 15.30. When the lower shear box moves laterally, shear failure of a rock specimen occurred along a small spacing between two rigid boxes.

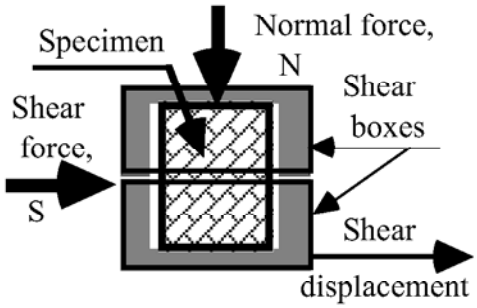

Fig. 15.30 Illustration of direct shear test

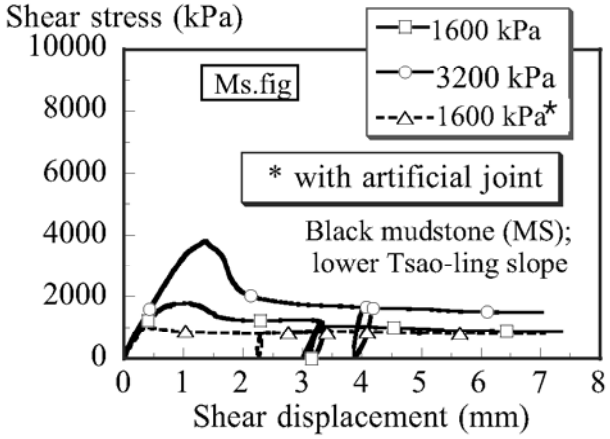

Fig. 15.31 Shear stress vs. shear displacement relationship of Tsaoling black mud stone

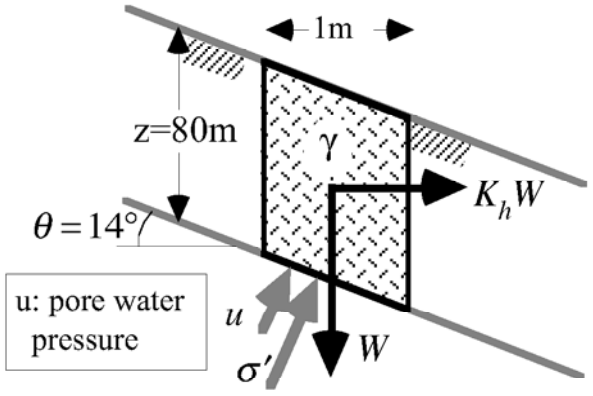

Fig. 15.32 Idea of quasistatic stability analysis

Figure 15.31 presents the drained direct shear results of black mud stone specimens collected from the slip plane. Two intact specimens under different confining pressures developed peak strengths which were then followed by softening and a state of residual strength (constant stress level). Cracking and shear failure occurred at and after the peak strength. One cycle of unloading and reloading in the residual state did not develop a peak strength again because the specimen with cracks had already lost the peak strength. Effects of existing cracks were considered significant in the slope failure in 1999 because the earthquakes in 1862 and 1941 not only caused slope failure but also probably produced cracks in the remaining part which failed in 1999. In this respect, a third test was run by combining two separate rock specimens with a smooth interface in between. The dashed curve in Fig. 15.31 indicates that there is no peak strength and that the residual strength is more or less similar to that of an intact specimen under the same pressure of 1600 kPa. Thus, the residual strength stands for the strength of cracks and weak interfaces.

A pseudostatic stability analysis was conducted by using the idea of an infinite slope subjected to static lateral force (Fig. 15.32). The seismic coefficient, $K_h = 0.305$, was obtained by substituting $A_{max} = 748$ Gal at a nearby CHY028 station (8 km from Tsaoling, Seismology Center of Central Weather Bureau) in an empirical formula (Sect. 12.3):

$$K_h = \sqrt[3]{A_{max}/g}/3. \quad (15.1)$$

For the residual strength, c = 417 kPa and ϕ = 19.4° were used. The derived safety factors were 1.01 for the peak strength and 0.73 for the residual strength.

A risk assessment of seismic slope failure requires evaluation of not only the factor of safety but also the travel distance of failed debris (Fig. 15.57). The latter issue certainly needs understanding of soil behavior in the course of rapid sliding movement. A unique idea on mechanism of long-traveling landslide was proposed by Sassa et al. (2004). This idea supposes that grains are crushed extensively in a thin layer (slip plane) during slope failure. Consequently, the granular structure of soil loses its capability to bear the overburden (loss of effective stress) and excess pore water pressure develops. This mechanism is called sliding surface liquefaction. This idea may also be applicable to a fault action if a fault is filled with soil.

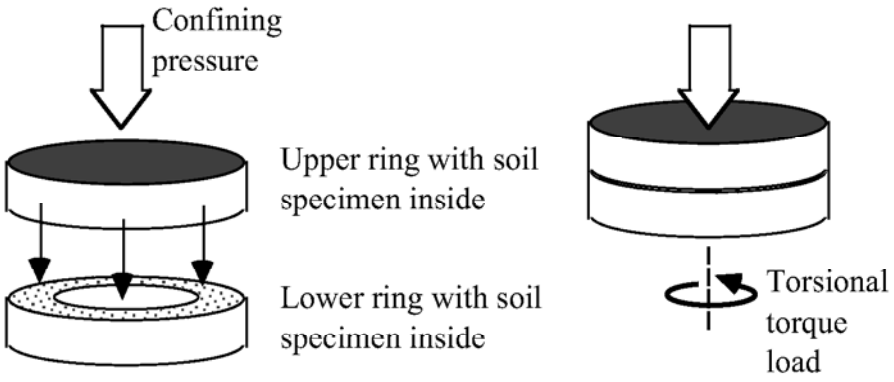

Fig. 15.33 Illustration of ring shear test

The role of sliding surface liquefaction has been studied experimentally by using a ring shear device. This device houses a hollow cylindrical soil specimen within upper and lower containers and applies torsional shear load. Since the specimen has a cylindrical shape, there is no limitation in shear displacement (Fig. 15.33). This feature is suitable in experimental reproduction of sliding surface mechanism in which slip displacement may be as large as tens of meters or more. Note that this device can measure shear displacement of a ring but cannot determine shear strain because strain is concentrated (localized) within a narrow sliding surface.

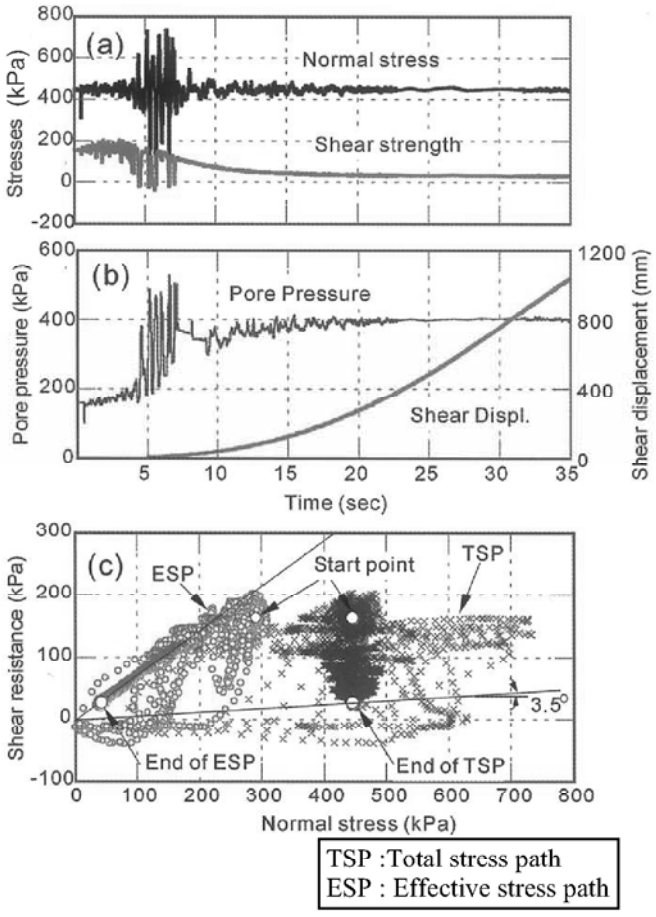

Fig. 15.34 Experimental reproduction of sliding surface liquefaction by means of ring shear device (after Sassa et al., 2004)

Figure 15.34 illustrates a typical test result in which the sliding displacement was induced in sand to be as large as 1,100 mm at a rate of about 50 mm/s. This rate corresponds to a real velocity of landslide mass. It is seen that cyclic loading of both shear and normal stresses increased the pore water pressure (Fig. 15.34b), and accordingly the shear strength decreased to a level of about 20 kPa (Fig. 15.34a). Since this strength was lower than the applied shear stress (vertical coordinate of Fig. 15.34c as well as the initial static shear stress of about 170 kPa), soil movement was accelerated and the displacement became as large as 1,100 mm. Note that the effective stress path (red symbols in Fig. 15.34c) shows that the stress path reached the failure line. Therefore, the development of large displacement is understandable. Nigawa landslide which was triggered

by the 1995 Kobe earthquake was studied by running a similar ring shear test (Sassa et al. 1996).

Crushing of sand grains was verified by observing the soil behavior through a transparent side wall. In Fig. 15.35a, individual grains were visible prior to shear. Once shear displacement started, the initial high effective stress (300 kPa) caused crushing and lots of sand powders emerged within the specimen (Fig. 15.35b).

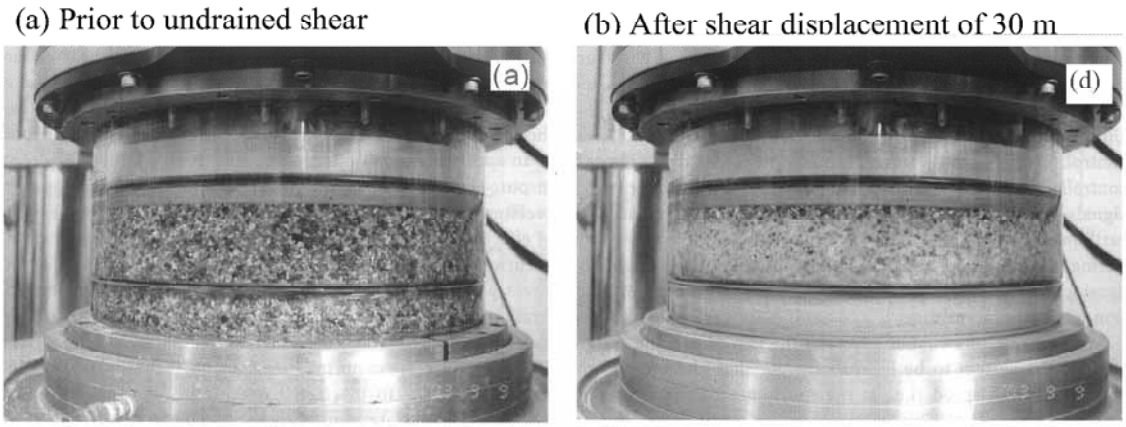

Fig. 15.35 Ring shear test with visual observation of grain behavior (Sassa et al., 2004)

Among many landslides in Taiwan, 1999, the second most gigantic one, second to the Tzaoling (Sect. 15.3), was the one at Jiu-Feng-Er-Shan. Its view from a helicopter is shown in Fig. 15.36. The exposed layer of gray color is probably made of shale stone which formed a slip plane (Fig. 15.37), similar to the slide at Tsaoling. Figure 15.38 shows a plantation of betel palm trees (檳榔樹) near the top of this slide. It is interesting that the tree and its root were separated from the ground, suggesting that the tree jumped out of the ground due to strong (but probably less than 980 Gal) vertical acceleration. Residents near the top of this slide say that they heard a roaring and explosive sounds during the slide. They also saw the sky had pink color during shaking in midnight.

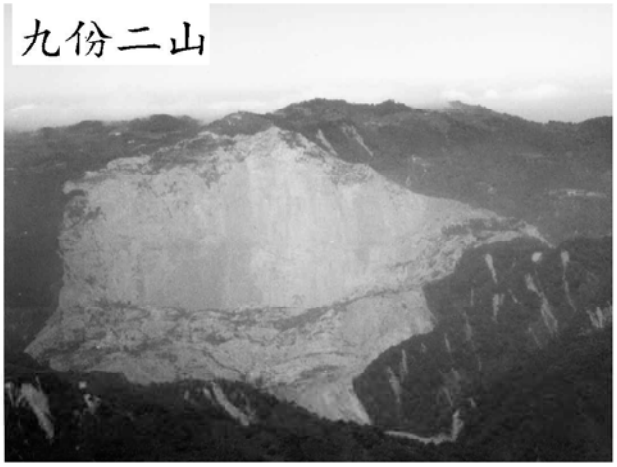

Fig. 15.36 Aerial view of Jiu-Feng-Er-Shan landslide

Fig. 15.37 View of Jiu-Feng-Er-Shan landslide

Fig. 15.38 Palm tree separated from ground

Fig. 15.39 Appearance of 99 peaks after the quake (Sino Geotechnology Inc., 1999)

Fig. 15.40 Gravelly material composing 99 peaks

Ninety-nine peaks (九九峰) developed many surface slides as well and lost vegetation (Fig. 15.39). This mountain was made of gravelly sand and was vulnerable to earthquake-induced falling down of the material. Figure 15.40 indicates the gravelly material at the top of one of the failed slope.

Seismic failure of natural slopes is a significant problem to human societies. It is therefore desired to inspect the stability of slopes near human habitations as much as possible. The stability analysis has to take into account the expected intensity of earthquake motion, topography of the studied slope, and material properties of the rock/soil. This process requires a time-consuming site investigation, and, therefore, it is costly and unlikely to be practiced everywhere. To avoid complexity, Fig. 15.41 shows relationship between the earthquake magnitude and the maximum epicentral distance of failed slopes during past earthquakes. Beyond this distance, slope failure is unlikely. Although significantly simplified, it can do some help to risk assessment.

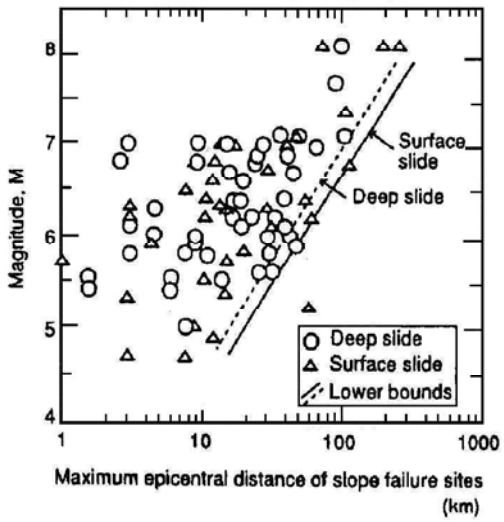

Fig. 15.41 Maximum possible epicentral distance to failed slopes during past earthquakes (Yasuda, 1993)

A slightly more detailed but time-consuming method has been proposed by the Kanagawa Prefectural Government (1986). This method counts points in accordance with site conditions, adds the points together, and assesses the magnitude of landslide risk of localities. Table 15.1 shows the counting of points, and Table 15.2 indicates the number of possible slope failures in a 500 m ×500 m square grid of localities. This type of work is called zoning and hazard assessment. The numbers in Table 15.1 were obtained by statistic analyses of past case studies. In particular, the small value of W_4 for soil may appear strange because it implies that soft soil slopes is more stable than hard rock slopes. This strange situation is due to the fact that failure of soil slopes is rare during earthquakes; slopes of softer materials are already destroyed prior to earthquakes by heavy rainfall etc.

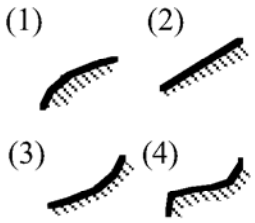

Fig. 15.42 Vertical cross section of slopes

This method is useful in quick assessment of local/regional risk of seismic landslides. It, therefore, does not show safety factor of any individual slope.

Table 15.1 Weighting for factors related to slope instability (Kanagawa Prefectural Government, 1986)

Factor	Category	Weight	Factor	Category	Weight
Maximum surface acceleration (Gal), W_1	0–200	0.0	Hardness of rock, W_4	Soil	0.0
	200–300	1.004		Soft rock	0.169
	300–400	2.306		Hard rock	0.191
	>400	2.754	Length of faults (m), W_5	No fault	0.0
Length of a contour line at mean elevation (m), W_2	0–1000	0.0		0–200	0.238
	1000–1500	0.071		>200	0.710
	1500–2000	0.320	Length of artificial slopes (m), W_6	0–100	0.0
	>2000	0.696		100–200	0.539
Difference between highest site and lowest site (m), W_3	0–50	0.0		>200	0.845
	50–100	0.550	Shape of slope, W_7 (see Fig. 15.42)	(1)	0.0
	100–200	0.591		(2)	0.151
	200–300	0.814		(3)	0.184
	>300	1.431		(4)	0.207

Table 15.2 Assessed number of slope instabilities (Kanagawa Prefectural Government, 1986)

$W=W_1+W_2+W_3+W_4+W_5+W_6+W_7$	2.93	3.53	3.68	
Rank	A	B	C	D
Number of slope failures within 500 m×500 m grid	0	1–3	4– 8	>9

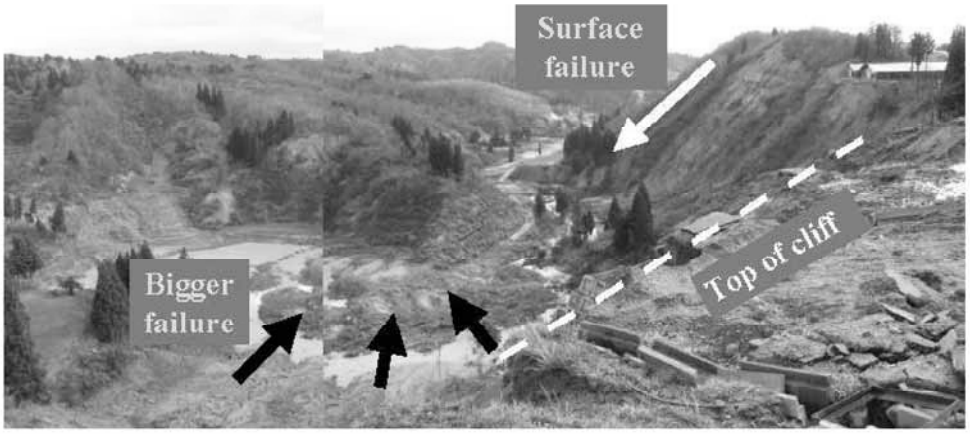

Fig. 15.43 Different extents of lateral movement of debris due to different volumes at Naraki after 2004 Chuetsu earthquake

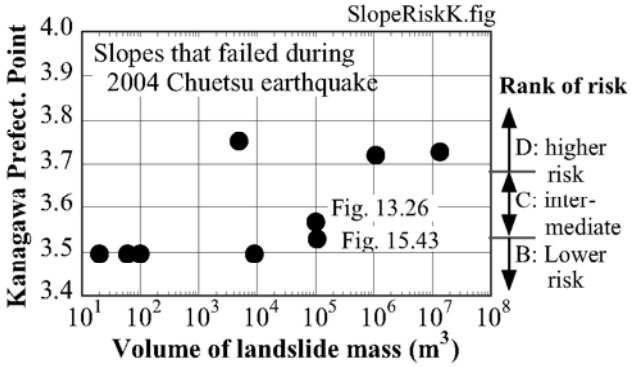

Fig. 15.44 Assessment of seismic risk of slopes by Kanagawa Prefecture method

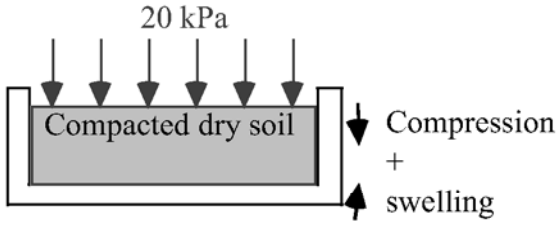

Fig. 15.45 Method of swelling test

As shown above, concerning the W_4 factor, the Kanagawa method does not fully account for local soil conditions. Moreover, the experience of many landslides during the 2004 Niigata Chuetsu earthquake revealed that the size of slope failure affected the extent of risk. Figure 15.43, for example, demonstrates two slope failures which occurred at a short distance from each other. The bigger one caused the debris to translate significantly in the lateral direction and stopped the stream flow, forming a natural dam (Sect. 15.3). The other one was merely falling of the surface weathered soil and the fallen material did not move laterally very much. Thus, it was thought necessary to add an assessment of "size" in the risk assessment. Another issue was the effect of water on slope instability because the Chuetsu earthquake was preceded by heavy rainfall three days before.

First, Fig. 15.44 plots the Kanagawa method´s point against the volume of landslide mass for many slope failures during the Chuetsu earthquake. Generally, there is a good consistency between the volume of landslide and the calculated point. There are, however, two slopes (Figs. 13.26 and 15.43) that received relatively low points in spite of their damage extent.

Effort was made to improve the method by paying attention to the effects of water on properties of local

soils (Mizuhashi et al. 2006). It was, however, considered difficult in practice to collect undisturbed soil samples and to run laboratory shear tests, because it was too elaborate for the present purpose of damage assessment. Therefore, disturbed soils were collected from the surface of failed slopes in the Chuetsu area and, in addition to measurement of liquid limits and plastic limits (Sect. 1.1), volume change upon water submergence was measured.

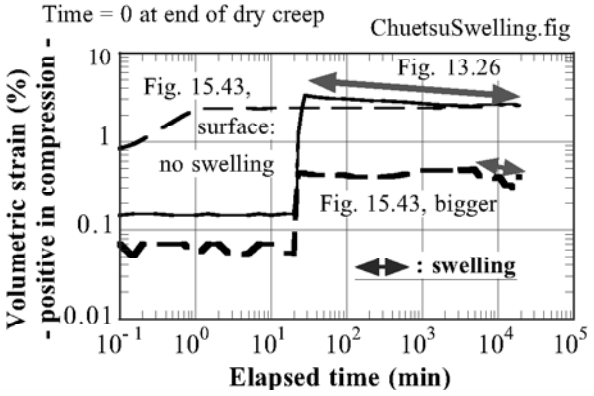

Fig. 15.46 Example of swelling tests (volume change after water submergence)

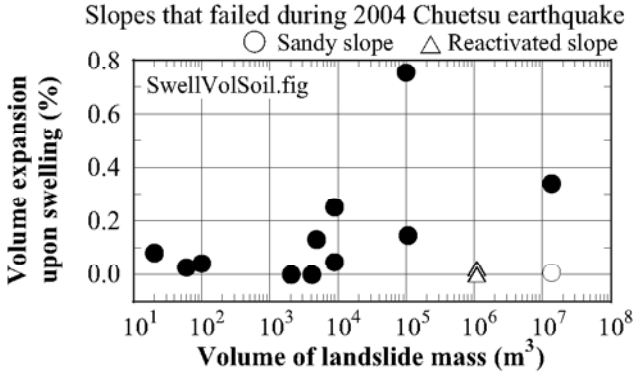

Fig. 15.47 Relationship between volume of slope failure and extent of soil swelling

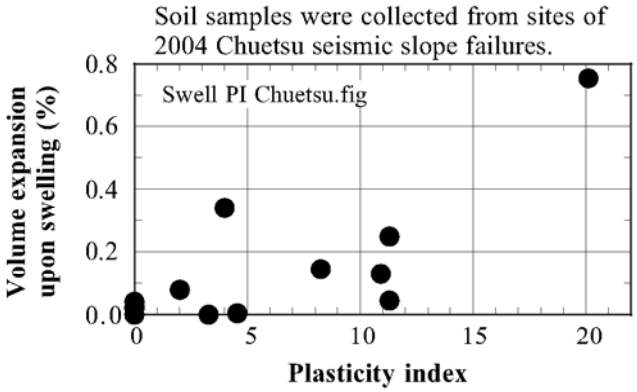

Fig. 15.48 Correlation between plasticity index and swelling strain

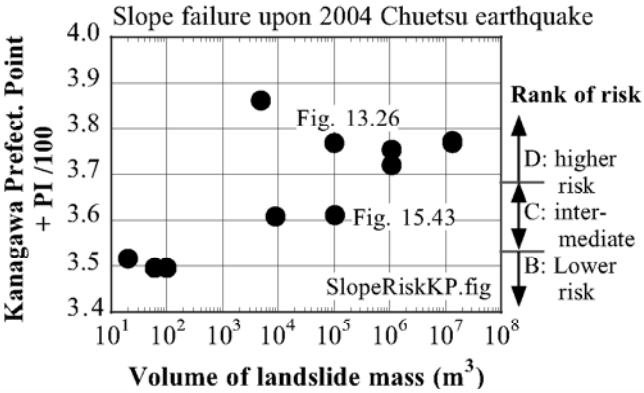

Fig. 15.49 Revisal of seismic risk assessment of slopes by means of plasticity index

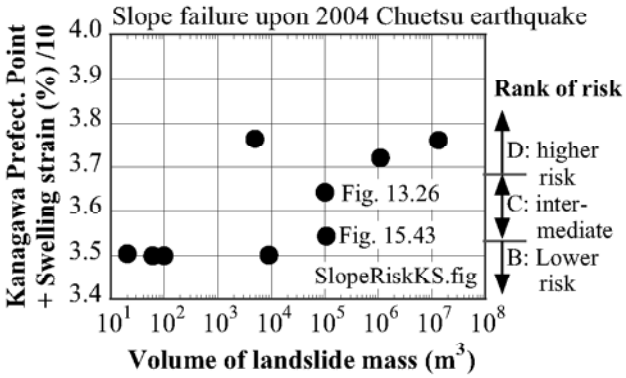

Fig. 15.50 Revisal of seismic risk assessment of slopes by means of swelling strain

Figure 15.45 illustrates the method of testing. First, an air-dry soil sample was prepared in a conventional oedometer (consolidation testing device) by compacting with a hammer with a constant and specified energy. After loading under 20 kPa and allowing for creep deformation in a dry state, water was introduced into the sample quickly. This water submergence caused subsidence, and thereafter, some soils exhibited swelling. It is supposed in this study that swelling is caused by interaction of clay mineral and water and leads to loss of shear strength. Figure 15.46 shows the time history of volume change of three specimens which are those in Fig. 13.26 and Fig. 15.43 (both bigger and surface ones). It is therein seen that the extent of swelling varies with soil types; the surface material in Fig. 15.43 did not have swelling.

Figure 15.47 shows a positive correlation between the volume of landslide mass and the measured volumetric strain during swelling. There are, however, exceptional cases where the material was sandy or the landslide was a reactivation of an existing unstable mass. These cases do not affect the significance of the swelling strain in practice.

One of the shortcomings in the use of swelling is the long time needed for the test (Fig. 15.45). To avoid this, a correlation between swelling strain and plasticity index was plotted in Fig. 15.48. There is certainly some relationship between them, and probably the plasticity index can be used as an alternative parameter which does not require much time for testing.

Figures 15.49 and 15.50 examine two types of revisal of the original Kanagawa Prefecture method. The original points were modified by adding either (plasticity index)/100 or (swelling strain, %)/10. It may be seen that points for the cases of Figs. 13.26 and 15.43 were increased to more reasonable values. This is particularly significant in the case of Fig. 15.49 wherein the plasticity index was employed for improvement.

Heezen and Ewing (1952) stated that a sequential breakage of submarine telegraph cables immediately after the 1929 Grand Banks earthquake in the continental slope to the south of New Foundland was caused by a turbidity current of water and mud. Figure 15.51 by Heezen et al. (1954) indicates that the slope inclination was as small as 1/500 or less in the area of submarine cable breaks, while the velocity of the turbidity current was on average 20 knots (=39 km/h); the highest velocity probably exceeded 90 km/h. It is remarkable that the fluidized debris traveled more than 700 km over a very small inclination of sea bed. Note, however, that Hasegawa and Kanamori (1987) stated that the ground shaking which was recorded at the time of the sliding was not of an earthquake origin, but was the consequence of huge submarine sliding. If this is correct, one should understand that the Grand Banks Sliding was caused by nonseismic causes (Sect. 15.8).

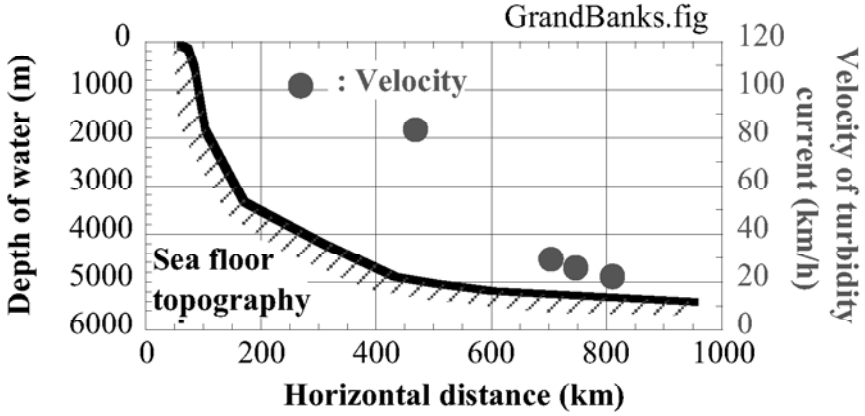

Fig. 15.51 Velocity of turbidity current after Grand Banks earthquake (drawn after Heezen et al., 1954)

Fig. 15.52 Conceptual sketch of Valdez submarine landslide (Drawn by David Laneville; after Coulter and Migliaccio, 1966)

Fig. 15.53 Aerial photograph of former site of Valdez (taken by K.Horikoshi)

A submarine landslide occurred in a gigantic scale at Valdez, Alaska, in March, 1964, when the great Alaska earthquake affected the area. Figure 15.52 illustrates the loss of sea slope, and the harbor facilities disappeared. The total volume of landslide was estimated to be around 100 million m^3 (Coulter and Migliaccio, 1966). Consequently, a large tsunami was produced and washed Valdez town. Figure 15.53 shows the aerial view of the present Valdez delta in 2002. The subsoil in this deltaic deposit consists of fine-grained cohesionless soil. This material was produced by scraping of mountain rock by glacier. Moreover, the small particle size makes the velocity of grain sedimentation very slow in water, and therefore the density becomes low. When the gigantic earthquake occurred in Alaska in 1964, this submarine slope failed easily, most probably accompanied by development of excess pore water pressure. This feature of glacier deposit is similar to that of tailing material (Sect. 20.5).

The Alaska earthquake also destroyed the sea-front ground in the town of Seward. Most probably, the shaking effect was superimposed by tsunami action (Lemke, 1971) which caused rapid drop of water level and loss of buoyancy force in soil.

Most probably, submarine landslides have been repeated in the past, although they were not detected because they were hidden by the sea-water coverage.

Another earthquake of magnitude = 6.7 induced a submarine landslide in the Mediterranean Sea off the coast of Orléansville (later called El Asnam and further renamed as Ech Cheliff), Argeria, in 1954. This slide traveled more than 70 km toward the deep sea (Heezen and Ewing, 1955) at a rate of, roughly, 40 km/h.

The body of a volcano is often affected by seismic motion. Figure 15.54 reveals an example in which a submerged wall of the Tohya (洞爺湖) caldera lake fell down at the time of the 1993 Hokkaido-Nansei-Oki earthquake and affected the shore line.

Fig. 15.54 Earthquake-induced failure of caldera wall (Tohya Lake, 1993)

15.8 Nonseismic Submarine Landslides

Submarine landslides have occurred at many places in the past. Terzaghi (1956) as well as Andresen and Bjerrum (1967) reported very unstable nature of submarine slopes and the typical example was taken of fjord deposits. An event at shore of Skagway in Alaska (1994) is one of the examples (Kulikov et al. 1996). Figure 15.55 illustrates their locations, inclusive of historic and prehistoric ones. Three important nonseismic causes of the submarine landslides are described below:

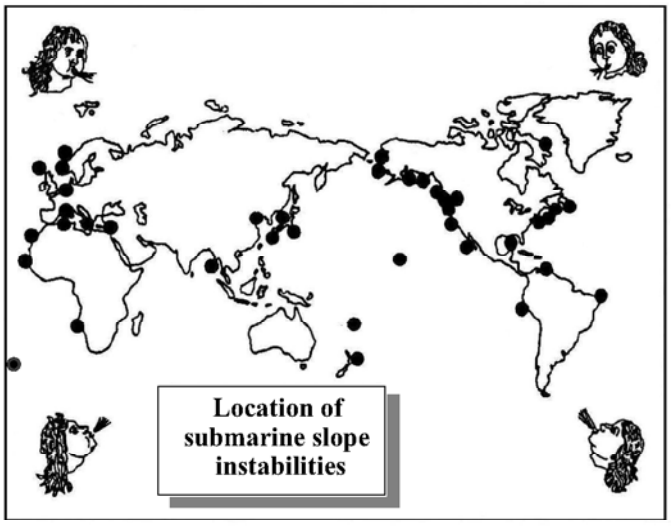

Fig. 15.55 Location of submarine landslides, historic and prehistoric

1. *Rapid sedimentation*: This is a major problem at mouths of big rivers where the rate of sedimentation is very rapid. Although the shear stress increases quickly together with sedimentation, the effective stress and shear strength take time for development due to delayed consolidation. Thus, the factor of safety decreases with time and minor impacts such as wave action or small earthquake suddenly trigger the total failure. An oil production platform was destroyed by this mechanism off the Mississippi River mouth (Sterling and Strohbeck, 1973). More detailed study is going on off the Fraser River delta, Canada (McKenna et al. 1992; Chillarige et al. 1997). Figure 15.56 is a small example of submarine landslide which was triggered by rapid sedimentation of sand in the sea bed off this beach.

Fig. 15.56 Small submarine landslide and missing beach due to rapid sedimentation (Naruto, Japan)

2. *Wave action*: Wave pressure on seabed is not uniform. Therefore, it can create cyclic shear stress in the seabed (Henkel, 1970). The consequent pore pressure increase can lead to loss of shear strength and slope failure (Okusa, 1985). This mechanism of loading can be fatal in a slope of rapid sedimentation as discussed above.
3. *Tsunami*: Slope instability may be induced by a rapid draw-down of water level in front of its face. This is because of the loss of buoyancy force which used to support the slope when the water level was higher. A typical example is the failure of the ongoing reclamation site of Nice Airport, France, where a tsunami was triggered by the massive movement of seabed sediment after its rapid deposition and the sea water level dropped (Seed et al. 1988).

A gigantic submarine landslide and a sudden change of submarine topography may trigger tsunami. Kulikov et al. (1998) pointed out that several nonseismic tsunami had occurred at the time of low tide. This is consistent with a well-known fact that rapid draw-down of reservoir water can trigger instability in shore slope. This instability is caused by the disappearance of buoyancy force after lowering of water level and the weight of the soil which still contains much pore water.

In addition to the aforementioned causes, Locat and Lee (2002) mentioned such causes as gas charging,

explosion of gas hydrate, low tides, seepage, glacial loading, and volcanic island growth. Among these, methane gas hydrate is an icy material which is buried in the soil of the ocean sea bottom (Matsumoto, 1997; Cruickshank and Masutani, 1999). It maintains stability under high pressure and/or low temperature. It is said that the seabed methane hydrate was less stable during the last glacier period when the sea level was lower than today by more than 100 m and the hydrate underwent lower pressure. A possible explosion of this material could have triggered submarine landslides of a huge scale (Ashi, 1999; Rothwell et al. 1998). One of the biggest submarine landslides in the prehistoric times is the Storegga Slide which occurred 30,000–50,000 years ago in the North Sea off Trondheim of Norway (Bugge et al. 1988). Its volume is estimated to be 3.88×10^{12} m^3. This event was probably triggered by unstable hydrate upon an earthquake (Bugge et al. 1988). Holcomb and Searle (1991) described several gigantic submarine landslides around volcanic islands such as Hawaii, Tristan da Cunha, and Canary.

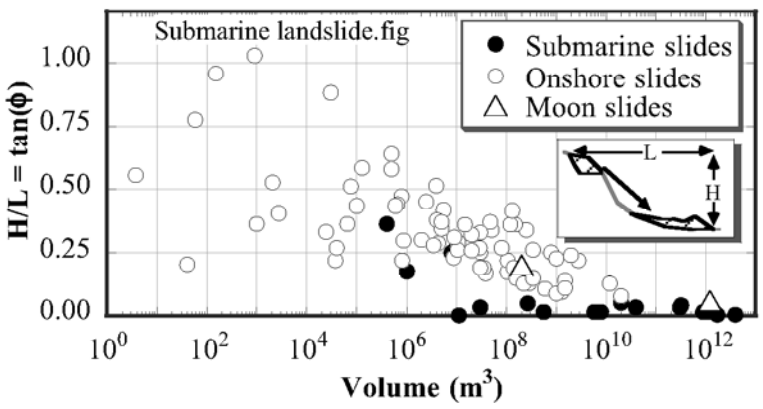

Fig. 15.57 Apparent frictional coefficient of landslides; subaerial and submarine

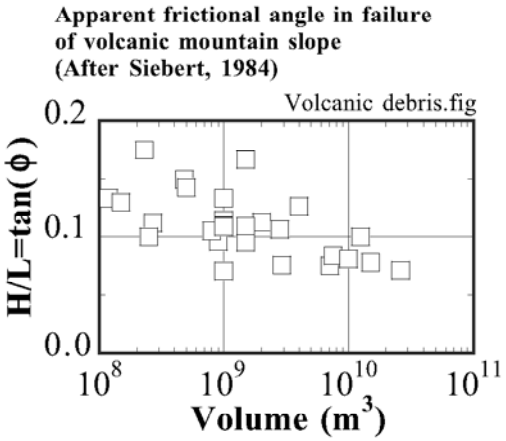

Fig. 15.58 Apparent frictional coefficient in failure of volcanic mountains (data by Siebert, 1984)

Upon submarine landslides, the energy dissipation of moving soil mass is approximately evaluated by using the height of fall, H, and the horizontal distance of flow, L. Consequently,

$$\phi = \arctan(H/L) \qquad (15.2)$$

is supposed to be the frictional angle of the flowing debris (Hsü, 1975); for its mathematical derivation, refer to Sect. 15.9. Figure 15.57, wherein data was collected from such literatures as Scheidegger (1973), Howard (1973), Moriwaki (1987) and Okuda (1984) as well as the author´s own study, indicates the frictional parameter, ϕ, thus obtained. Note that, first, the subaerial (on-shore) landslides have a greater friction than the submarine ones, and second that the greater volume of flowing soil mass is associated with smaller friction. Therefore, the greater landslide can reach a longer distance. Noteworthy is that the apparent frictional angle is significantly small in large submarine slides probably because of the high degree of water saturation and pore pressure development (liquefaction).

Figure 15.57 suggests that typically $H/L = \tan30° \approx 0.6$ for the cases of smaller debris volume which often occurs. This information is frequently used for assessment of area which is vulnerable to potential risk of landslide (hazard mapping). Note, however, that there are cases where H/L is very small possibly due to high water content and development of excess pore water pressure in the soil mass. It is empirically known, furthermore, that debris flow in volcanic slopes (Fig. 15.4 for example) has smaller H/L and greater travel distance than other onshore events (Siebert, 1984); compare Fig. 15.58 with Fig. 15.57.

15.9 Derivation of Formula for Apparent Frictional Angle

This section presents the mathematical derivation of the formula on friction angle (15.2) which was proposed by Hsü (1975). Figure 15.59 illustrates a slope and a moving mass at its surface. This mass is an idealization of debris and the frictional angle between this mass and the slope surface is designated by ϕ. Note that the present discussion is based on a total stress approach of soil mechanics. Hence, the shear force, S, is related to the normal force, N, without paying attention to effective stress or pore water pressure;

$$\text{Friction } S = N \tan\phi = mg \cos\theta \tan\phi, \qquad (15.3)$$

where θ stands for the slope angle at the current location of the moving mass. The energy dissipation per unit time due to friction is expressed as

$$\frac{dD}{dt} = S \times \text{velocity} = mg \cos\theta \tan\phi \times \frac{ds}{dt}, \qquad (15.4)$$

where s is the location of the moving mass measured along the slope surface (Fig. 15.59).

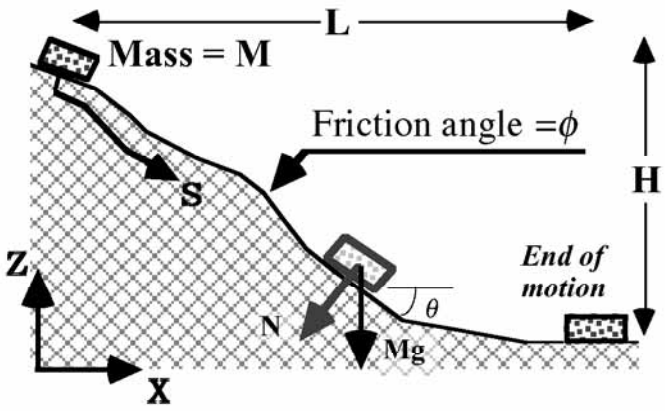

Fig. 15.59 Motion of mass along slope surface

Fig. 15.60 Changed flow direction of debris at bottom of slope (rainfall-induced slope failure in Shikoku, Japan, in 2004)

By integrating (15.4) from the beginning to the end of motion, the total energy dissipation is obtained and it is equal to the loss of gravity potential energy. Hence,

$$mgH = \int \frac{dD}{dt} dt = \int S \times \text{velocity}\, dt = \int mg \cos\theta \tan\phi \times \frac{ds}{dt} dt. \qquad (15.5)$$

Since $\cos\theta = \dfrac{dx}{ds}$,

$$H = \tan\phi \times \int \frac{dx}{ds}\frac{ds}{dt} dt = \tan\phi \times \int \frac{dx}{ds} ds = \tan\phi \times \int dx = \tan\phi \times L. \qquad (15.6)$$

Consequently,

$$\frac{H}{L} = \tan\phi. \qquad (15.7)$$

Theoretically, this formula assumes a two-dimensional straight channel of flow. When the flow channel in a valley is bent and three-dimensional (Fig. 15.60), energy is dissipated by collision between soil mass and valley wall. Also, it is difficult to define L.

Figure 15.61 demonstrates the biggest onshore landslide that can be seen today (Harrison and Falcon, 1938). The width and the length of this Seimareh, Iran, landslide are 16 km and 5 km, respectively, while the thickness of the failed rock mass is 300 m (Fig. 15.62). Thus, the total volume of the debris was around 24 billion m^3. A C_{14} dating (Watson and Wright, 1969) by using sediment of a lake in this area suggests that this landslide occurred 10,000 years ago. Since the annual precipitation is very low (500–600 mm/year; van Zeist and Bottema, 1977), erosion is not significant and it is possible to see the slip plane (Fig. 15.63). This slide was probably caused by erosion by river at the foot of the slope (Oberlander, 1965). It is however possible that the unstable slope was finally destroyed by shaking. As Fig. 15.57 implied, this huge volume of debris makes H/L value very small; the travel distance was as long as 20 km which is evidenced by the debris deposit which is still visible today (Fig. 15.64).

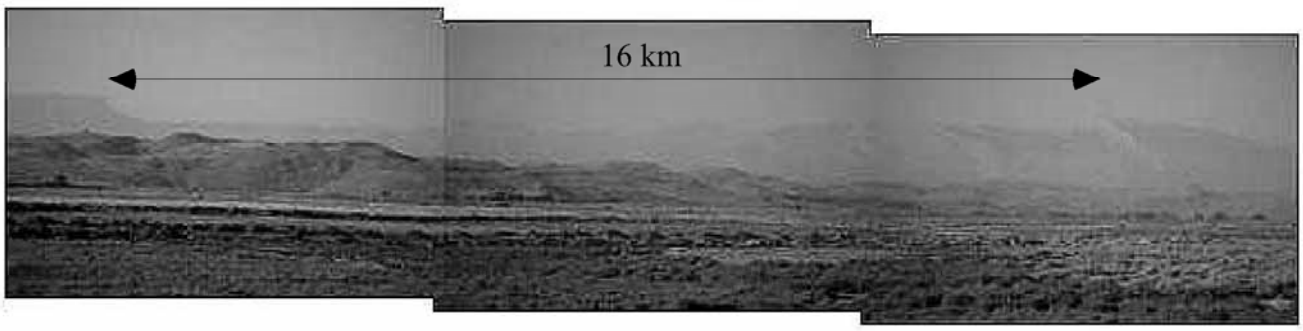

Fig. 15.61 Total view of Seimareh landslide seen from nearby town of Pol-e-Doghtar

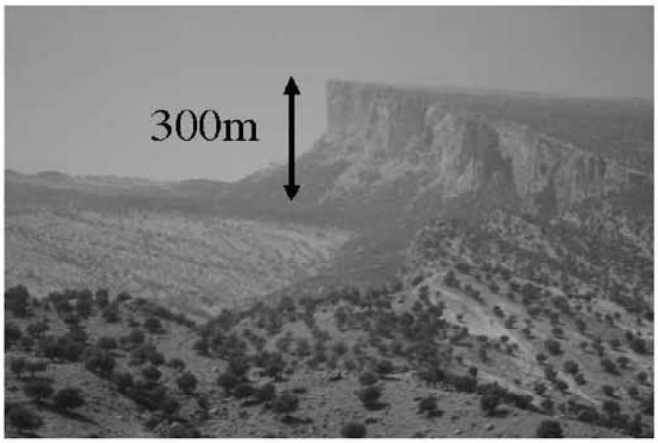

Fig. 15.62 Side cliff of Seimareh landslide

Fig. 15.63 Smooth slip plane of Seimareh landslide

Fig. 15.64 Debris deposit of Seimareh landslide

List of References in Chapter 15

Andresen, A. and Bjerrum, L. (1967) Slides in subaqueous slopes in loose sand and silt, Marine Geotechnique, Ed. A.F. Richards, Univ. Illinois Press, pp. 221-239.
Ashi, J. (1999) Large submarine landslides associated with decomposition of gas hydrate, Landslide News, Vol. 12, pp. 17-20.
Bugge, T., Belderson, R.H. and Kenyon, N.H. (1988) The Stregga Slide, Phil. Trans. Roy. Soc. London, A. 325, pp. 357-388.
Chillarige, A.V., Morgenstern, N.R., Robertson, P.K. and Christian, H.A. (1997) Seabed instability due to flow liquefaction in the Fraser River delta, Can. Geotech. J., Vol. 34, pp. 520-533.
Coulter, H.W. and Migliaccio, R.R. (1966) Effects of the earthquake of March 27, 1964 at Valdez, Alaska, Professional Report 542-C, US Geological Survey.
Cruickshank, M.J. and Masutani, S.M. (1999) Methane hydrate research & development, Sea-Technology, Vol. 40, No. 8, pp. 69-74.
Harrison, J.V. and Falcon, N.L. (1938) An ancient landslip at Saidmarreh in southwestern Iran. J. Geol., Vol. 46, pp. 296-309.
Hasegawa, H.S. and Kanamori, H. (1987) Source mechanism of the magnitude 7.2 Grand Banks earthquake of November 1929: double couple or submarine landslide?, Seismol. Soc. Am. Bull., Vol. 77, pp. 1984–2004.
Hayakawa, A. (1967) Photograph of Mt. Huascaran, Mountains of the World, YAMAKEI Color Guide 8, p. 177 (in Japanese) (早川滉 撮影 山渓カラーガイド 8, 山と渓谷社).
Heezen, B.C. and Ewing, M. (1952) Turbidity currents and submarine slumps, and the 1929 Grand Banks Earthquake, Am. J. Sci., No. 250, pp. 849–873.
Heezen, B.C. and Ewing, M. (1955) Orleansville earthquake and turbidity currents, Bull. Am. Assoc. Petroleum Geologists, Vol. 39, No. 12, pp. 2505–2514.
Heezen, B.C., Ericson, D.B. and Ewing, M. (1954) Further evidence for a turbidity current following the 1929 Grand Banks earthquake, Deep-Sea Research, Vol. 1, pp. 193–202.
Henkel, D.J. (1970) The role of waves in causing submarine landslides, Geotechnique, Vol. 20, No. 1, pp. 75-80.
Holcomb, R.T. and Searle, R.C. (1991) Large landslides from oceanic volcanoes, Marine Geotechnol., Vol. 10, pp. 19-32.
Howard, K.A. (1973) Avalanche mode of motion: Implication from Lunar examples, Science, Vol. 180, pp. 1052-1055.
Hsü, K.J. (1975) Catastrophic debris streams (Sturzstroms) generated by rockfalls, Geol. Soc. Am. Bull., Vol. 86, pp. 129-140.
Imaizumi, F., Tsuchiya, S. and Ohsaka, O. (2005) Behaviour of debris flows located in a mountainous torrent on the Ohya landslide, Japan, Can. Geotech. J., Vol. 42, pp. 919–931.
Ishihara, K. (1985) Stability of natural deposits during earthquakes, Theme Lecture, 11th ICSMFE, San Francisco, Vol. 1, pp. 321–376.
Ishihara, K., Haeri, S.M., Moinfar, A.A., Towhata, I. and Tsujino, S. (1992) Geotechnical aspects of the June 20, 1990 Manjil Earthquake in Iran, Soils Found., Vol. 32, No. 3, pp. 61–78.
Kanagawa Prefectural Government (1986) Prediction of seismic damage in Kanagawa Prefecture, pp. 13–63 (in Japanese).
Kawata, S. (川田三郎) (1943) Study of new lake created by the earthquake in 1941 in Taiwan 台南州斗六郡草嶺震生湖, Bulletin of the Earthquake Research Institute, University of Tokyo, 東京大学地震研究所彙報, Vol. 21, pp. 317–325 (in Japanese).
Keefer, D.K. (1984) Landslides caused by earthquakes, Geol. Soc. Am. Bull., Vol. 95, pp. 406–421.
Kulikov, E.A., Rabinivich, A.B., Thompson, R.E. and Bornhold, B. (1996) The landslide tsunami of November 3, 1994, Skagway Harbour, Alaska, J. Geophys. Res., Vol. 101, No. C3, pp. 6609-6615.
Kulikov, E.A., Rabinivich, A.B., Fine, I.V., Bornhold, B. and Thompson, R.E. (1998) Tsunami generation by landslides at the Pacific coast of North America and the role of tides, Oceanology, Vol. 38, No. 3, pp. 323-328.
Lemke, R.W. (1971) Effects at Seward, In The Great Alaska Earthquake of 1964, Chapter on Geology, National Academy of Sciences, Washington , D.C., pp. 395–437.

Locat, J. and Lee, H.J. (2002) Submarine landslides: advances and challenges, Can. Geotech. J., Vol. 39, pp. 198-212.
Matsumoto, R. (1997) Perspective of methane hydrate science, J. Jpn. Inst. Energy, Vol. 76, No. 841, pp. 354-361.
McKenna, G.T., Luternauer, J.L. and Kostaschuk, R.A. (1992) Large-scale mass-wasting event on the Fraser River, British Columbia, Can. Geotech. J., Vol. 29, pp. 151-156.
Mizuhashi, M., Towhata, I., Sato, J. and Tsujimura, T. (2006) Examination of slope hazard assessment by using case studies of earthquake- and rainfall-induced landslides, Soils Found., Vol. 46, No. 6, pp. 843–853.
Moriwaki, H. (1987) A prediction of the runout distance of a debris, J. Jpn. Landslide Soc., Vol. 24, No. 2, pp. 10-16 (in Japanese).
Oberlander, T. (1965) The Zagros Streams, Syracuse Geographical Series, No. 1, Syracuse University Press.
Okuda, S. (1984) Features of debris deposits of large slope failures investigated from historical records, Report of Disaster Prevention Research Institute, Kyoto University, No. 27B-1 (in Japanese).
Okusa, S. (1985) Wave-induced stresses in unsaturated submarine sediments, Geotechnique, Vol. 35, No. 4, pp. 517-532.
Plafker, G., Ericksen, G.E. and Fernández Concha, J. (1971) Geological aspects of the May 31, 1970, Peru Earthquake, Bull. Seismol. Soc. Am., Vol. 61, No. 3, pp. 543–578.
Rothwell, R.G., Thompson, J. and Kähler, G. (1998) Low-sea-level emplacement of a very large late Pleistocene 'megaturbidite' in the western Mediterranean Sea, Nature, Vol. 392, pp. 377-380.
Sassa, K., Fukuoka, H., Scarascia-Mugnozza, G. and Evans, S. (1996) Earthquake-induced-landslides: distribution, motion and mechanisms, Soils Found., Special Issue on Geotechnical Aspects of the January 17 1995 Hyogoken-Nambu earthquake, pp. 53–64.
Sassa, K., Fukuoka, H., Wang, G.-H. and Ishikawa, N. (2004) Undrained dynamic-loading ring-shear apparatus and its application to landslide dynamics, Landslides, Vol. 1, No. 1, pp. 7–19.
Scheidegger, A.E. (1973) On the prediction of the reach and velocity of catastrophic landslides, Rock Mech., Vol. 5, pp. 211-236.
Seed, H.B., Seed, R.B., Schlosser, F., Blondeau, F. and Juran, I. (1988) The Landslide at the Port of Nice on October 16 1979, EERC Report 88-10, University of California, Berkeley.
Siebert, L. (1984) Large volcanic debris avalanches: characteristics of source areas, deposits, and associated eruptions, J. Volcanol. Geothermal Res., Vol. 22, pp. 163-197.
Sino Geotechnology Inc. (1999) Taiwan Chi-Chi earthquake 9.21. 1999, ISBN 957-99763-2-5.
Sterling,G H. and Strohbeck, E.E. (1973) The Failure of the South Pass 70 Platform B in Hurricane Camill, Proc. Offshore Technology Conf., Vol. 2, pp. 719-729.
Tabata, S., Mizuyzma, T. and Inoue, K. (2002) Natural dam and disasters, Kokin Shoin Publ., ISBN4-7722-5065-4 C3051, pp. 50–53 (in Japanese).
Terzaghi, K. (1956) Varieties of submarine slope failures, Harvard Soil Mechanics Series, No. 52.
Towhata, I., Yamazaki, H., Kanatani, M., Ling, C.-E. and Oyama, T. (2002) Laboratory shear tests of rock specimens collected from site of Tsao-ling earthquake-induced landslide, Tamkang J. Science Eng., Vol. 4, No. 3, pp. 209–219.
van Zeist, W. and Bottema, S. (1977) Palynological investigations in Western Iran, Palaeohistoria, Vol. 19, pp. 20–85.
Voight, B. and Elsworth, D. (1997) Failure of volcano slopes, Geotechnique, Vol. 47, No. 1, pp. 1–31.
Watson, R.A. and Wright Jr., H.E. (1969) The Saidmarreh landslide, Iran, Geological Society of America Special Paper 123, pp. 115–139.
Yasuda, S. (1993) Zoning for slope instability, Manual for zonation on seismic geotechnical hazards, Technical Committee 4, Int. Soc. Soil Mech. Found. Eng., p. 49.